Polarons in highly doped atomically thin graphitic materials

J. P. Hague
The Open University, Walton Hall, Milton Keynes, MK7 6AA, United Kingdom
(Received 13 July 2011; revised manuscript received 9 July 2012; published 10 August 2012)

Polaron spectral functions are computed for highly doped graphene-on-substrate and other atomically thin graphitic systems using the diagrammatic Monte Carlo technique. The specific aim is to investigate the effects of interaction on spectral functions when the symmetry between sublattices of a honeycomb lattice has been broken by the substrate or ionicity, inducing a band gap. Introduction of electron-phonon coupling leads to several polaronic features, such as band-flattening and changes in particle lifetimes. At the K point, differences between energies on each sublattice increase with electron-phonon coupling, indicating an augmented transport gap, while the spectral gap decreases slightly. Effects of phonon dispersion and long-range interactions are investigated, and found to lead to only quantitative changes in spectra.

DOI: 10.1103/PhysRevB.86.064302 PACS number(s): 73.22.Pr

I. INTRODUCTION

The graphene hexagonal lattice leads to exceptional electronic properties: a zero band gap semiconductor with very high mobilities, and essentially massless Dirac fermions.[1] This has already led to a number of applications, but transistors for digital applications remain elusive because they require a gap. While a gap cannot be induced in suspended monolayer graphene, recent experimental work using angle resolved photoemission spectroscopy (ARPES) has shown that there may be band gaps in graphene on certain substrates: ARPES measurements have found a gap in graphene on a monolayer of intercalated gold on ruthenium[2] and there has been significant debate regarding whether a gap is present in monolayer graphene on silicon carbide.[3,4]

The debate about the existence of the gap seen for graphene on SiC relates to the interpretation of ARPES measurements.[5] The authors of Ref. 3 claim that there is a gap of around 0.26 eV because of modulation of the potential due to the substrate; however, it has been claimed that this gap is a misinterpretation of other excitations such as polarons and polaritons.[4,6] ARPES measurements are carried out using either doping or gating to move the system away from half filling. For example, in Ref. 3 the Fermi energy, E_F is shifted by around 0.4 eV. Bostwick *et al.*[4] consider a system where E_F is shifted by 0.45 eV. Where evidence has been found for the opening of the gap in the ruthenium system due to a breaking of the symmetry of the two carbon sublattices in graphene, the Fermi energy was reported to be around 0.15 eV below the Dirac point.[2] Therefore, the effects of doping on spectral functions are of interest.

An alternative material with a honeycomb lattice and a band gap resulting from a modulated potential is boron nitride (BN), which can be mechanically exfoliated in atomically thin layers.[7] Atomically thick hexagonal BN (h-BN) bonds through sp_2 hybridization (just as in graphene) and has itinerant electrons in π orbitals.[8] In BN, ionicity means that π orbitals on N sites are shifted up in energy by $+\Delta$, with a decrease in energy of $-\Delta$ on B sites, causing a gap of order 2Δ. *Ab initio* simulations have established hopping in the BN monolayer to be $t = 2.33$ eV[9] and that the parameter, $\Delta = 1.96$ eV $= 0.84t$. Experiments on monolayer h-BN find a gap of 5.56 eV.[10] Longitudinal acoustic (LA) phonon energies peak at around 140 meV at the M point, and transverse acoustic (TA) phonons at around 110 meV at the K point. Optical phonon energies range between 160 meV and 200 meV,[11] and strong coupling between electrons and phonons is expected because individual sites have a net charge in the ionic materials.

Several other atomically thin materials can be mechanically exfoliated, including SnS_2, CdI_2, and MoS_2, but these have the chalcogenide structure, rather than the graphene honeycomb lattice. Other layered materials that have a honeycomb structure include GaN, which has a band gap of 2.15 eV and can be grown in thin films.[12] The related AlN can also exist in a hexagonal structure with band gap 6.28 eV.[13] Following the discovery of silicene,[14] it is possible that other III-V semiconductors can be encouraged to grow in thin hexagonal films.

Recently, I calculated that gaps caused by modulated potentials on honeycomb lattices may be enhanced by introducing strong electron-phonon coupling through a highly polarizable superstrate.[15,16] Effective electron-electron interactions can be induced via a strong interaction between the electrons in a graphene monolayer and phonons in a strongly polarizable substrate because of limited out of plane screening, similar to that seen for quasi-2D materials.[17] Such interactions have been experimentally demonstrated between carbon nanotubes and a SiO_2 substrate,[18] and are necessary to account for the lower mobilities of graphene on SiO_2.[19] These interactions will form polaronic states and affect the overall electronic structure in the graphene monolayer. For the graphene-on-substrate systems with small gaps, devices could be covered with highly polarizable superstrates to combine gap effects with strong electron-phonon interaction.

No work has previously been carried out to establish the properties of polarons in a gapped graphene system, and this paper discusses how spectral functions for a single electron could be affected by electron-phonon interactions, as an approximation to polaronic effects in the highly gated or doped regime. I calculate the effects of electron-phonon interaction on electrons in a honeycomb lattice (graphene) where a gap has been opened with a modulated potential. I present results computed using the numerically exact diagrammatic quantum Monte Carlo (DQMC) technique, and compute spectral functions using stochastic analytic inference. The

DQMC method used here is valid for a single polaron—that is a single electron at the bottom of an empty band interacting with a cloud of phonons. So, results presented in this paper are approximately valid in the heavily doped regime, well away from half filling. The paper is organized as follows. The model Hamiltonian is introduced in Sec. II. Details of the extensions to DQMC specific to graphene are explained in Sec. III. Section IV presents detailed spectral functions for a range of model parameters. A summary and conclusions are given is Sec. V.

II. MODEL HAMILTONIAN

In this section, I introduce details of a model Hamiltonian for polaronic effects in gapped systems. Three components are required to examine polaronic interactions between graphene and surface phonons in a substrate (or superstrate): (a) intersite hopping within the hexagonal plane, which is well known to properly account for the band structure of monolayer graphene, (b) an electron-phonon interaction to account for any polaronic effects from interaction with surface phonons in the substrate, and (c) direct Coulomb interaction between the electrons and substrate. The same components are valid for monolayers of ionic graphitic materials such as BN.

A complication of the Hamiltonian required to describe graphene is that a basis of two atoms is needed to represent the honeycomb lattice. This leads to a Hamiltonian with the form

$$H_{\text{tb}} = \sum_{\boldsymbol{k}} (\phi_{\boldsymbol{k}} a^{\dagger}_{\boldsymbol{k}} c_{\boldsymbol{k}} + \phi^{*}_{\boldsymbol{k}} c^{\dagger}_{\boldsymbol{k}} a_{\boldsymbol{k}}), \tag{1}$$

$$H_{\text{e-ph}} = \sum_{\boldsymbol{kq}} g_{\boldsymbol{q}} [c^{\dagger}_{\boldsymbol{k}-\boldsymbol{q}} c_{\boldsymbol{k}} (d^{\dagger}_{\boldsymbol{q}} + d_{-\boldsymbol{q}}) + a^{\dagger}_{\boldsymbol{k}-\boldsymbol{q}} a_{\boldsymbol{k}} (b^{\dagger}_{\boldsymbol{q}} + b_{-\boldsymbol{q}})] + \tilde{g}_{\boldsymbol{q}} [a^{\dagger}_{\boldsymbol{k}-\boldsymbol{q}} a_{\boldsymbol{k}} (d^{\dagger}_{\boldsymbol{q}} + d_{-\boldsymbol{q}}) + c^{\dagger}_{\boldsymbol{k}-\boldsymbol{q}} c_{\boldsymbol{k}} (b^{\dagger}_{\boldsymbol{q}} + b_{-\boldsymbol{q}})], \tag{2}$$

$$H_{\text{ph}} = \sum_{\boldsymbol{q}} \Omega_{\boldsymbol{q}} (b^{\dagger}_{\boldsymbol{q}} b_{\boldsymbol{q}} + d^{\dagger}_{\boldsymbol{q}} d_{\boldsymbol{q}}), \tag{3}$$

$$H_{\text{static}} = \sum_{i\sigma} V(\boldsymbol{r}_i) n_{i\sigma}. \tag{4}$$

Here, H_{tb} is the tight binding Hamiltonian representing the kinetic energy of the electrons in the graphene monolayer, $\phi_{\boldsymbol{k}} = -t \sum_i \exp(i\boldsymbol{k} \cdot \boldsymbol{\delta}_i)$, where $\boldsymbol{k}$ is the electron momentum and $\boldsymbol{\delta}_i$ are the nearest neighbor vectors from A to B sublattices, $\boldsymbol{\delta}_1 = a(1,\sqrt{3})/2$, $\boldsymbol{\delta}_2 = a(1,-\sqrt{3})/2$, and $\boldsymbol{\delta}_3 = (-a,0)$. Electrons are created on A sites with the operator $a^{\dagger}_i$ and B sites with $c^{\dagger}_i$.

The term $H_{\text{e-ph}}$ describes the electron-phonon interaction. Phonons with momentum $\boldsymbol{q}$ are created on A sites with $b^{\dagger}_{\boldsymbol{q}}$ and on the B sublattice with $d^{\dagger}_{\boldsymbol{q}}$. Thus interactions between electrons and phonons on the same sublattices have magnitude $g_{\boldsymbol{q}}$, and interactions between different sublattices have magnitude $\tilde{g}_{\boldsymbol{q}}$. The Fröhlich form for the electron-phonon interaction has been demonstrated experimentally for carbon nanotubes on SiO_2,[18] is theoretically proposed for quasi-2D systems where out of plane hopping is low,[17] and has also been found necessary to account for mobilities for graphene on substrate systems.[19] The interactions between electrons in the graphene and polarizable ions in the substrate are shown schematically in Fig. 1. There are only weak interactions between electrons and phonons within the graphene plane, accounting for the very high mobility of suspended graphene. In ionic materials such as BN, in plane interactions may be stronger. Two interactions are considered: a Holstein interaction, where the Fourier transform of the force function is momentum independent and $\tilde{g} = 0$, and a Fröhlich interaction, where the Fourier transform $g_{\boldsymbol{q}} = \sum_{\boldsymbol{n}} g_0[\boldsymbol{n}] e^{i\boldsymbol{q}\cdot\boldsymbol{n}}/\sqrt{N}$ of the force function is truncated at nearest neighbors so $\tilde{g}_{\boldsymbol{q}} \propto \sum_i \exp(i\boldsymbol{q} \cdot \boldsymbol{\delta}_i)$.

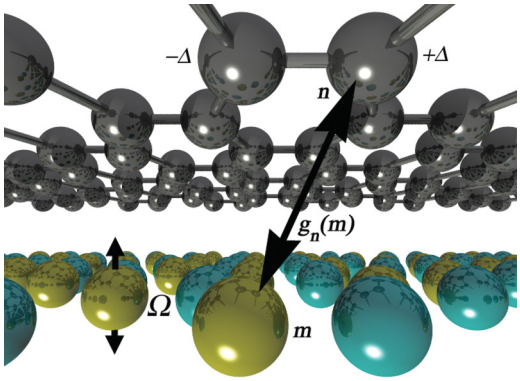

FIG. 1. (Color online) Graphene-substrate system annotated with interactions and sublattices. Electron-phonon interactions between the graphene layer and substrate are poorly screened, and large interactions are possible.

H_{ph} is the energy of the phonons in the substrate (treated as harmonic oscillators, and including both kinetic and potential energy of the ions), and the phonon dispersion is $\Omega_{\boldsymbol{q}} = \Omega + \Delta\Omega[\cos(q_x\sqrt{3}) + 2\cos(q_y\sqrt{3}/2)\cos(3q_x/2)]$, where $\Delta\Omega$ controls the width of the phonon band. It is usual to define a dimensionless electron-phonon coupling, $\lambda = \Phi(0,0)/tM\Omega^2$, where the effective interaction $\Phi(\boldsymbol{n},\boldsymbol{n}') = \sum_{\boldsymbol{m}} g_{\boldsymbol{m}}[\boldsymbol{n}] g_{\boldsymbol{m}}[\boldsymbol{n}']/(2M\Omega)$, where $g_{\boldsymbol{m}}[\boldsymbol{n}] = \kappa/(1 + |\boldsymbol{n} - \boldsymbol{m}|^2)^{3/2}$ and κ is a coupling constant. Typical effects of the electron-phonon interaction in conventional semiconductors are the generation of polarons, leading to changes in the band structure and thus the effective mass of the carriers, modification of the Landau levels and changes in the optical properties of the material such as absorption peaks in the mid infrared.

To complete the model of graphene on a substrate, H_{static} describes interaction between electrons in the monolayer and a static potential, $V(\boldsymbol{r}_i)$, induced by the substrate (where $\boldsymbol{r}_i$ are vectors to lattice sites). Here, a modulated potential is considered where A sites have energy Δ and B sites $-\Delta$ leading to breaking of the symmetry between A and B sublattices and giving rise to a gap. Such a form has been suggested to explain gaps in graphene on SiC[3] and graphene on rubidium,[2] and is the standard form used in tight binding models of BN.[9] A similar electron-phonon Hamiltonian without the static potential was considered by Covaci and Berciu.[20]

Solution of this Hamiltonian is extremely involved, with complications arising because electron-phonon interactions

are retarded. The next section describes how to solve the polaron problem for the graphene lattice using DQMC.

III. METHOD: DIAGRAMMATIC QUANTUM MONTE CARLO

I use the diagrammatic quantum Monte Carlo (DQMC) method to establish the properties of polarons on the graphene lattice.[21,22] In order to take account of the bipartite lattice and AB modulated potential, the DQMC method has to be modified to include basis. This is achieved by considering the noninteracting Green function to have a matrix form. A slight complication is presented by the off-diagonal terms of this matrix, which are complex. This could in principle lead to a phase problem (which is a generalized sign problem). The complex phase is found to be very small when measuring the on-site Green functions of interest here. For imaginary time, $\tau_f > \tau_i$ and at absolute zero, the Green functions are defined as follows:

$$\mathbf{G} = \begin{pmatrix} G_{AA} & G_{AB} \\ G_{BA} & G_{BB} \end{pmatrix} \tag{5}$$

$$= \begin{pmatrix} -\langle a(\tau_f)a^\dagger(\tau_i)\rangle & -\langle a(\tau_f)c^\dagger(\tau_i)\rangle \\ -\langle c(\tau_f)a^\dagger(\tau_i)\rangle & -\langle c(\tau_f)c^\dagger(\tau_i)\rangle \end{pmatrix}, \tag{6}$$

where

$$G_{AA} = \frac{[\exp(-E_B(\tau_f-\tau_i)) + \exp(-E_A(\tau_f-\tau_i))]}{2} + \frac{\Delta[\exp(-E_A(\tau_f-\tau_i)) - \exp(-E_B(\tau_f-\tau_i))]}{2\sqrt{|\phi_k|^2+\Delta^2}}, \tag{7}$$

$$G_{BB} = \frac{[\exp(-E_B(\tau_f-\tau_i)) + \exp(-E_A(\tau_f-\tau_i))]}{2} + \frac{\Delta[\exp(-E_B(\tau_f-\tau_i)) - \exp(-E_A(\tau_f-\tau_i))]}{2\sqrt{|\phi_k|^2+\Delta^2}}, \tag{8}$$

$$G_{AB} = \frac{\phi_k[\exp(-E_B(\tau_f-\tau_i)) - \exp(-E_A(\tau_f-\tau_i))]}{2\sqrt{|\phi_k|^2+\Delta^2}}, \tag{9}$$

$$G_{BA} = \frac{\phi_k^*[\exp(-E_B(\tau_f-\tau_i)) - \exp(-E_A(\tau_f-\tau_i))]}{2\sqrt{|\phi_k|^2+\Delta^2}}, \tag{10}$$

$E_A = \mu + \sqrt{\Delta^2+|\phi_k|^2}$, and $E_B = \mu - \sqrt{\Delta^2+|\phi_k|^2}$. Here, the pseudochemical potential μ allows greater control of the algorithm, but since a single particle is simulated, the true chemical potential lies at the bottom of the band. Thus the results are only accurate when the electron density is low (i.e., the system is doped well away from half-filling). For $\tau_f < \tau_i$ and absolute zero, all Green functions are zero valued because the polaron only contains a single electron. Since $G(\tau_f < \tau_i) = 0$, vertices are ordered between times 0 and τ, where τ is the length of the diagram.

In its most basic form, the algorithm proceeds by inserting and removing interaction lines into or from the electron propagator. The propagators for the Holstein interaction with local phonons have the form $\exp(-\Omega_q\tau)\delta_{XX}$ where $X \in \{A,B\}$ represents the sublattice type at the end of the propagator and δ_{XX} is the Kronecker δ function. Sublattice type is fixed at the ends of the whole diagram so that the dynamics of each symmetry broken sublattice can be probed independently.

The imaginary time Green function tails off exponentially, and can vary by several orders of magnitude, which makes direct measurement of the Green function histogram impossible within a reasonable time scale. To avoid this, a Wang-Landau algorithm is used to make an initial guess for the histogram, so that all diagram lengths τ are visited a similar number of times during each simulation. The advantage of the Wang-Landau algorithm is that it obtains the histogram extremely fast. This histogram is not used directly for computation of the Green function, because the bin size is finite leading to systematic errors. Rather, it is used as input for a reweighting procedure so that all imaginary times are visited[22] and the τ dependent Green function is calculated using the estimator given in Ref. 22 which corrects for finite histogram bin size. Proper choice of the pseudochemical potential, μ, speeds up the initialization of the Wang-Landau algorithm.

It is worth noting that G_{AB} and G_{BA} have a complex phase. A Monte Carlo procedure can be obtained by keeping track of this phase $e^{i\theta}$ such that averages of an estimator O are given by $\langle e^{i\theta}O\rangle/\langle e^{i\theta}\rangle$. For all cases considered here, the average phase $\langle e^{i\theta}\rangle$ is found to be extremely close to 1, and no expectation values had a complex component after averaging. There is no obvious reason why the phase should cancel (unlike in the 1D case where the signs exactly cancel)[23] and, for large numbers of particles, the phase could become a problem.

In order to obtain spectral functions, stochastic analytic inference is used.[24] Green functions are built up from δ functions that can be moved continuously in frequency using a separate Monte Carlo update scheme. The ability to construct spectral functions from continuous frequencies is necessary to obtain reliable analytic continuation at absolute zero where features can be very sharply peaked. Each configuration of the spectral function is weighted as $w \propto \exp(-\chi^2/2\alpha)$ and the factor α is reduced from a large value until the average $\chi^2 < N_G$, the number of points in the Green function. Averages are then taken. Additional global updates (where all points can be shifted simultaneously) have been included in the procedure to ensure that the algorithm is ergodic.

IV. RESULTS

This section begins by examining how the opening of a band gap affects the spectral functions when the electron-phonon coupling is switched on. The phonon energy is set as $\hbar\Omega = t$ unless otherwise specified. This very high value is chosen so that features relating to polarons can be distinguished easily. Note that phonons of this energy are still in the adiabatic regime at around one-third of the half bandwidth. Naturally, this energy is much higher than that of any phonons in graphene

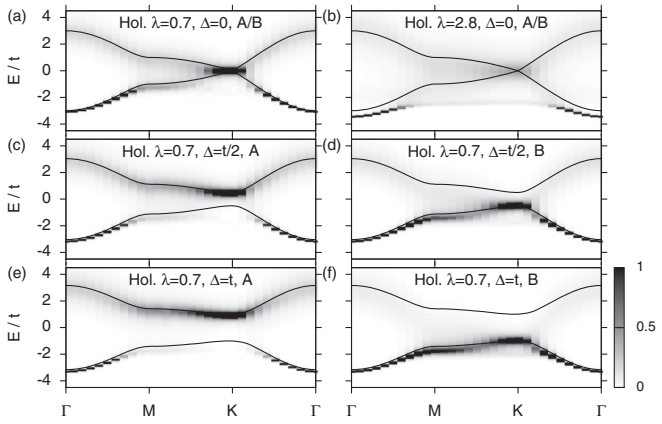

FIG. 2. Image plots of the graphene spectral function across the Brillouin zone. Various Δ and λ are shown. The noninteracting dispersion is overlaid. At $\Delta = 0$, A and B sublattices are symmetrical, leading to identical spectral functions, so only a single panel is shown for each λ. Comparison with the noninteracting dispersion shows that there is some flattening of the band close to the K point. The spectral function is sharp close to the K point. In the vicinity of the Γ point, the spectral function is also sharp for states within an energy $\hbar\Omega$ of the bottom of the band. Quasiparticle lifetime (related to the inverse of the width) is greatly reduced close to the tops of the bands. Increase in Δ breaks the AB symmetry. Some band flattening is seen. There is also a weak excitation associated with B sites at higher energies, which touches the lower band. Panel (a) $\Delta = 0$, $\lambda = 0.7$, (b) $\Delta = 0$, $\lambda = 2.8$ where A and B site electrons are identical. (c) and (d) $\Delta = 0.5t$, $\lambda = 0.7$, and (e) and (f) $\Delta = t$, $\lambda = 0.7$, showing A and B site electrons, respectively. There is only a single electron, so the chemical potential is at the bottom of the band, E_0. The origin is arbitrary, but for consistency has been taken as the point where the unperturbed bands cross.

or BN, or of any surface phonons in the substrate, and smaller values will also be discussed later in the paper. Values for Δ ranging from 0 to t are also large for the same reason. For simplicity (unless specified) the out-of-plane interaction g_{kq} is approximated to be momentum independent, and $\tilde{g} = 0$, leading to a local Holstein interaction.

Figure 2 shows how the graphene spectral function, $A(E)$, changes across the Brillouin zone. Spectral functions are computed from the full Green functions, $\mathcal{G}_{AA}(\tau)$ and $\mathcal{G}_{BB}(\tau)$, with $\mathcal{G}$ calculated on a logarithmic mesh with 500 points. Separate image plots can be seen for A and B type electrons to make the specific contributions from each sublattice clear, and the noninteracting band structure is superimposed for comparison. A moderate dimensionless electron-phonon coupling of $\lambda = 0.7$ is chosen, with the exception of panel (b), which shows spectral functions for the larger $\lambda = 2.8$. Panels (a) and (b) correspond to $\Delta = 0$, (c) and (d) to $\Delta = t/2$, and (e) and (f) to $\Delta = t$.

The main features of Fig. 2 are as follows. (1) The quasiparticle peaks are sharp at low energies $E - E_0 \lesssim \hbar\Omega$ (where E_0 is the polaron ground state energy) but broaden significantly for higher energies. This is especially noticeable in panels (a), (d), and (f). (2) A clearly identifiable polaron band (split off from the main dispersion) can be seen for large λ in panel (b). (3) Asymmetry between electrons on site A and site B increases with Δ. (4) The spectral gap can be seen to increase with Δ. The spectral gap is slightly smaller than Δ due to broadening of the quasiparticle peak. (5) The beginnings of a flat polaron band can be seen for $\Delta = t$ in panel (f) and is just visible in panel (d) for $\Delta = t/2$. Again, it should be noted that these results are for polarons (a single electron at the bottom of an empty band interacting with phonon modes). As the Fermi energy is changed, the spectral function close to the chemical potential may be modified significantly. Far from the chemical potential, differences should be less pronounced. Here, the spectral gap is defined as the distance between the peaks of the spectral function close to the Dirac point.

When $\Delta = 0$, A and B sites are symmetrical and the spectral function for each sublattice is identical, so results are only shown for the A sublattice in Figs. 2(a) and 2(b). In the vicinity of the Γ point, the spectral function is sharply peaked for states within an energy of around $\hbar\Omega$ of the bottom of the band, and quasiparticle lifetime (related to the inverse of the width) is greatly reduced for the highest energy states close to the tops of the bands. This is a polaronic effect: within an energy $\hbar\Omega$ of the bottom of the band the electrons have insufficient energy to excite real phonons. At the top of the band, the spectral functions are broad due to quasiparticle decays induced by interactions.

The spectral function is also sharply peaked close to the K point. By examining the zero gap states [Figs. 2(a) and 2(b)] it is possible to consider whether it is possible that polaronic states could simulate a gap. Examination of Fig. 2(a) shows that there is a flattening of the dispersion near the K point (highlighted by comparison with the noninteracting dispersion) accompanying a decrease in the width of the quasiparticle peak. The flattening of the dispersion close to the K point is associated with a steepening of the dispersion along the KM and KΓ lines, giving the dispersion the appearance of a waterfall. The waterfall-like features are at variance with the idea that polaronic features could look like a band gap,[6] since emulation of a gap would require the dispersion to show the opposite shape to that seen here: a very steep band structure close to K with a rapid change of gradient leading to flattening between K and M. Panel (b) shows that the spectral weight gets broader with increased λ, indicating that it is also likely that finite quasiparticle lifetimes contribute to an obscuring of any gap rather than any apparent gap opening. Since the results are taken with the chemical potential at the bottom of the band, the results are speculative and further studies at higher densities would be required to reach a full conclusion.

A major feature in panel (b) for $\lambda = 2.8$ is the emergence of a flat polaron band, which separates off from the lower band. Such a feature typically corresponds to the energy required to excite a real phonon, and is singular in basic Migdal-Eliashberg theories of electron-phonon interactions (see, e.g., Ref. 25). The large electron-phonon coupling leads to a significant decrease in the quasiparticle lifetime at large energies; however, the band flattening seen around the K point (which is unconnected to the polaron band) persists. The ground state polaron energy is lowered due to the polaron self-interaction (seen as the offset from the noninteracting band at the Γ point).

Increase in Δ breaks the symmetry between A and B sublattices, and this can be seen in Fig. 2, panels (c)–(f). A gap opens as Δ is increased. A band at high energies, roughly

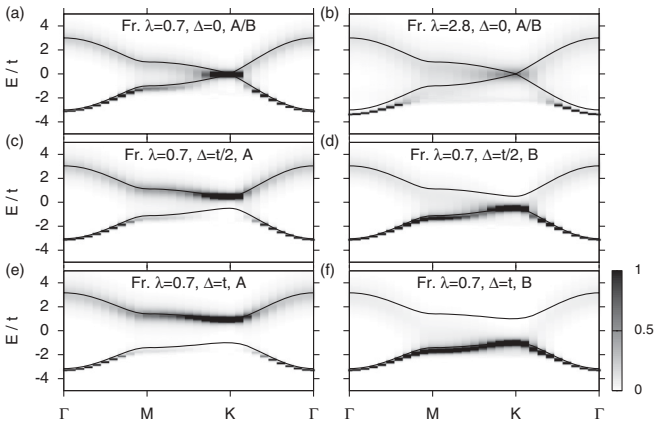

FIG. 3. Same as Fig. 2 with the leading nearest neighbor corrections from Fröhlich interactions included. There are only minor changes to the results.

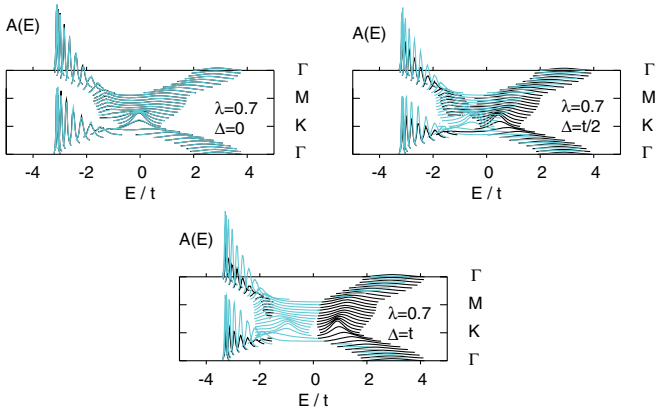

FIG. 4. (Color online) Variation of the graphene spectral function across the Brillouin zone for various Δ and $\lambda = 0.7$. The same data as Fig. 2 is shown with both A and B sublattices superimposed on the same plot. From top to bottom, $\Delta = 0$, $\Delta = t/2$, and $\Delta = t$. The gap opening is clearly visible. Broadening of the spectral functions can be seen, especially at larger energies.

tracing the dispersion of the ungapped, noninteracting band, can be seen in panels (d) and (f), although its spectral weight is extremely small. The origins of this band are unclear. Increased Δ also leads to a flat polaron band that separates from the main band (it can be seen as the lowest energy feature at the K point). This feature is only just visible in panel (d), but is clearly separated from the main band in panel (f). The appearance of this band at weak λ is a consequence of polaron localization at large Δ, which increases polaron self-interaction (i.e., the effective λ is increased by the localization).

To demonstrate that the effects are not artifacts of the local Holstein interaction, Fig. 3 shows the spectral functions computed for interactions that include nearest neighbor forces, the leading correction to the Fröhlich interaction. (N.B. Sums associated with the Fourier transforms of the force functions are truncated so that they are not prohibitively computationally expensive. A truncated near neighbor interaction contains sufficient physics to obtain good agreement with the full interaction).[26,27] The plots are qualitatively similar to those in Fig. 2. The main difference is that the longer range forces slightly reduce the effects of interactions at a particular λ: for the Fröhloich interaction, there is slightly less drop in the ground state energy of the polaron band, and the flat features appear at slightly higher energies relative to the bottom of the band. The slight increase in the width of the polaron band occurs because the distortions associated with the Fröhlich polaron are already preformed before the electron hops between sites, so the effective mass is smaller. The differences between Holstein and Fröhlich interactions are more pronounced for larger interaction strengths, as can be seen by comparing the $\lambda = 2.8$ results.

To clarify the effects of interaction and bare gap on the spectral function, Fig. 4 shows the same data, but with both spectral function types superimposed on the same plot. For clarity, spectral weight below a cutoff of less than 0.1 is not shown (variations on this order of magnitude are not distinguishable below this scale, and the resulting curve appears as a series of straight horizontal lines obscuring the plots). From top to bottom $\Delta = 0$, $\Delta = t/2$, $\Delta = t$, and $\lambda = 0.7$ in all panels. The gap opening can clearly be seen. The effects of interaction, which increases the width of the spectral function at large energies (where real phonons can be created), is much clearer in these plots.

Figures 5 and 6 show how the graphene spectral function changes across the Brillouin zone when the electron-phonon coupling is varied and $\Delta = t$ (from top to bottom, $\lambda = 0.7$, 1.4, 2.1, and 2.8). Spectral functions for the A sublattice can be seen on the left of Fig. 5 [panels (a), (c), (e), and (g)] and spectral functions for the B sublattice are shown on the right-hand side of the plot [panels (b), (d), (f), and (h)]. Self-interactions lower the polaron energy, and it can be seen that spectral weight at the Γ point moves to lower energies relative to the noninteracting bands as λ increases. At large λ, a sharply defined polaron band separates from the main band, and can be seen as a low energy band that is almost flat and has a high quasiparticle lifetime (again, this is the singular band found in conventional Migdal-Eliashberg theories). The remnant of the

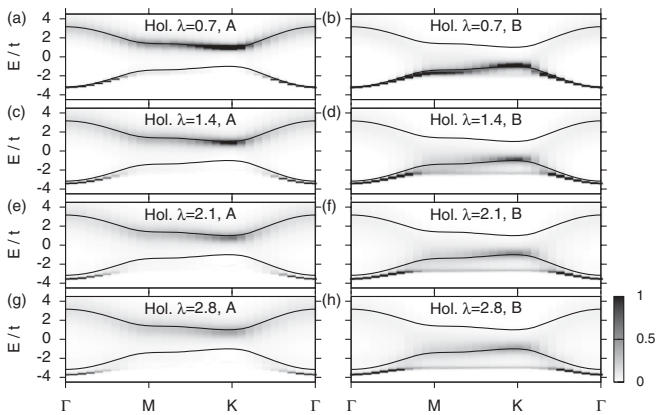

FIG. 5. Image plots of the graphene spectral function across Brillouin zone. $\Delta = t$ and various λ. Panels (a) and (b) $\lambda = 0.7$, (c) and (d) $\lambda = 1.4$, (e) and (f) $\lambda = 2.1$, and (g) and (h) $\lambda = 2.8$. A sites can be seen on the left and B on the right. A flat polaron band can be seen forming at an energy around $\hbar\Omega$ above the bottom of the band for very large λ. The quasiparticle lifetime decreases dramatically with increased λ.

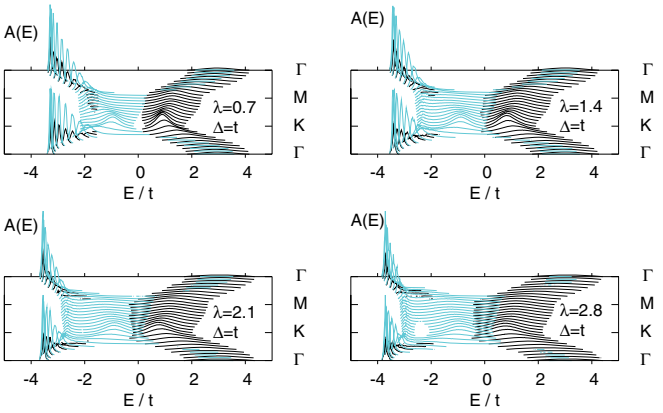

FIG. 6. (Color online) Graphene spectral function across Brillouin zone. $\Delta = t$ and various λ. Data is as Fig. 5 but with results for both sublattices plotted together. It can be seen that the gap is robust against increase in λ, although a number of additional excitations appear.

noninteracting band is visible as a sideband above the polaron band. The quasiparticle lifetime decreases dramatically with increased λ, seen as a broadening of the spectral function. A shadow band can be seen in the spectral functions for B sites, although it is relatively weak, and decreases in weight as λ is increased. Examination of Fig. 6 (which shows spectral functions for both sublattices superimposed onto the same plot) shows that the spectral gap is robust against increase in λ, although a number of additional excitations appear. Again, for completeness, the effects of longer range interactions are shown in Fig. 7. For the larger bare band gaps, the effects of interaction range are extremely small for all values of λ.

Finally, Fig. 8 shows how the spectral function at the K point evolves as the electron-phonon coupling is increased. Three main peaks are visible: (1) the lowest corresponds to the polaron band, (2) electrons on the A sublattice have at least one excited state, and (3) B type electrons can be seen at the highest energies.

In the strongly doped system, the gap between the A excited state and the B electron energy is essentially unchanged by an increase in the electron-phonon coupling, with the gap

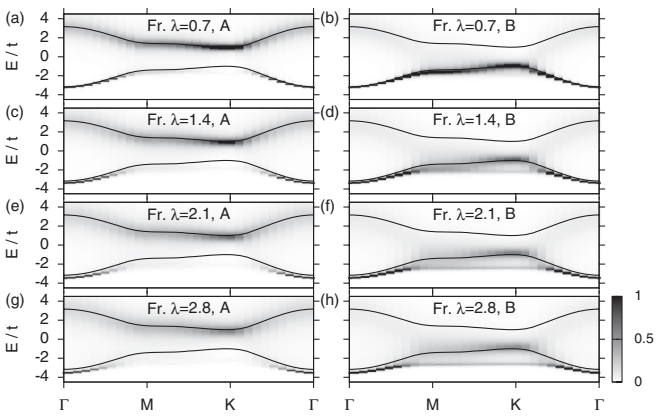

FIG. 7. Same as Fig. 5 with the leading corrections from Fröhlich interactions included. There are only moderate changes to the results, consistent with a small reduction in effective λ.

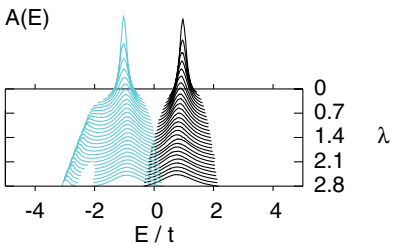

FIG. 8. (Color online) Graphene spectral function at the K point. $\Delta = t$ and λ is varied. The spectral gap (seen at approximately $E = 0$) is robust. The spectral functions broaden with increased λ, and the polaron band rapidly drops in energy leading to an enhanced transport gap.

remaining robust. The polaron band can be seen splitting off from the noninteracting band, with the polaron energy dropping rapidly at small λ, followed by a sustained decrease. This is related to the flattening of the polaron band seen in Fig. 5. As the electron-phonon coupling is increased, the quasiparticle lifetime drops, seen as a broadening of the peak. There is an increase in the energy difference between the bottom of the A band and the bottom of the B band at the Dirac point, indicating an increase in the potential barrier formed by the higher energy A sites. This indicates an increased transport gap at the K point from electron-phonon interactions, consistent with perturbation theory calculations at half filling.[23] Here, transport gap is taken to be the difference between the lowest energy states on A and B sublattices.

Finally, I consider the effects of lower phonon frequencies, dispersive phonons, and smaller bare band gaps in Fig. 9. In the figure, $\lambda = 2.8$ throughout. The truncated Fröhlich interaction is used in all panels. Comparison of panels (a) and (b) with panels (c) and (d) shows that including dispersive phonons with a half bandwidth of approximately 30% of the phonon frequency has no qualitative effect on the spectral functions. Far more important is the decrease in phonon frequency. At this large value of lambda, the sharp flat feature dissipates, and all features are generally broadened [panels (e) and (f)]. Again,

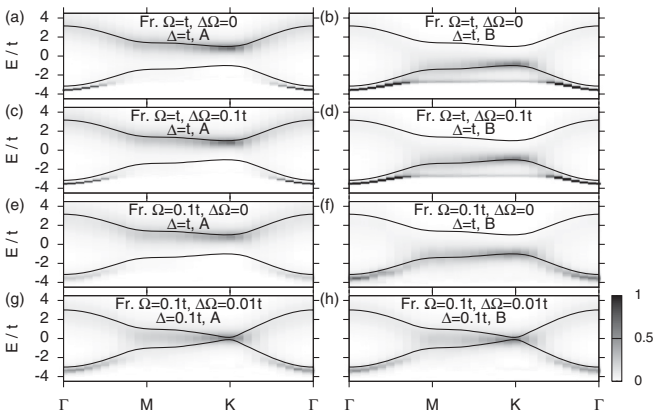

FIG. 9. Effects of dispersion, $\Delta\Omega$, and phonon frequency, Ω, on the spectral function. $\lambda = 2.8$ throughout. Broadening the phonon dispersion has no major effects on the spectral function. On the other hand, decreasing the phonon frequency leads to a broadening of all features corresponding to a sharp decrease in quasiparticle lifetime, and indicating a significant increase in scattering.

the inclusion of phonon dispersion causes no major changes in the spectral function. Reduction in Δ when $\Omega = 0.1t$ leads to the spectral functions shown in panels (g) and (h).

V. SUMMARY AND CONCLUSIONS

In this paper, I have used the diagrammatic quantum Monte Carlo technique to compute the spectral functions of polarons on a honeycomb lattice in the presence of a substrate or superstrate. Extensions to DQMC were introduced to deal with the bipartite honeycomb (graphene) lattice. Spectral functions were obtained for a variety of electron-phonon coupling strengths and substrate induced sublattice symmetry breaking using stochastic analytic inference. The results presented here relate to heavily doped graphene.

Electron-phonon interactions are seen to have a range of effects on the band structure. The quasiparticle peaks are sharp at low energies $E - E_0 < \hbar\Omega$, but broaden significantly for higher energies. A clearly identifiable polaron band with large quasiparticle lifetime forms. Asymmetry between electrons on different sublattices increases with Δ.

Flattening of the band around the K point in the absence of sublattice symmetry breaking suggests that electron-phonon coupling could not emulate a gap in the absence of a modulated potential. Spectral gaps induced by substrates are seen to be reasonably robust against interactions at heavy doping, although a shortening of quasiparticle lifetime (broadening of the spectral function) may make the gap difficult to discern.

A gap in the spectral function is induced on increase of the energy difference between sublattices, Δ, but is slightly reduced by broadening of the quasiparticle peak at large λ. The formation of a polaron band on increase of electron-phonon coupling increases the transport gap at the K point due to an increase in the energy difference between sublattices. This provides additional evidence that strongly polarizable substrates and superstrates could be used to enhance transport gaps opened by a substrate. Further work is underway to examine spectral functions and gaps close to half filling.

ACKNOWLEDGMENTS

I am pleased to acknowledge EPSRC Grant No. EP/H015655/1 for funding and useful discussions with P. E. Kornilovitch, A. S. Alexandrov, M. Roy, P. Maksym, E. McCann, V. Fal'ko, E. Burovski, N. J. Mason, N. S. Braithwaite, and A. Davenport.

[1] A. H. C. Neto, F. Guinea, N. M. R. Peres, K. S. Novoselov, and A. K. Geim, Rev. Mod. Phys. **81**, 109 (2009).
[2] C. Enderlein, Y. S. Kim, A. Bostwick, E. Rotenberg, and K. Horn, New J. Phys. **12**, 033014 (2010).
[3] S. Y. Zhou, G.-H. Gweon, A. V. Fedorov, P. N. First, W. A. D. Heer, D.-H. Lee, F. Guinea, A. H. C. Neto, and A. Lanzara, Nat. Mater. **6**, 770 (2007).
[4] A. Bostwick, T. Ohta, T. Seyller, K. Horn, and E. Rotenberg, Nature Phys. **3**, 36 (2007).
[5] It is also worth noting that the physics of the graphene on SiC system may be complicated because of the nature of the surface reconstruction, Y. Qi, S. H. Rhim, G. F. Sun, M. Weinert, and L. Li, Phys. Rev. Lett. **105**, 085502 (2010).
[6] E. Rotenberg, A. Bostwick, T. Ohta, J. L. McChesney, T. Seyller, and K. Horn, Nat. Mater. **7**, 258 (2008).
[7] K. Novoselov, D. Jiang, F. Schedin, T. J. Booth, V. V. Khotkevich, S. V. Morozov, and A. K. Geim, Proc. Natl. Acad. Sci. USA **102**, 10453 (2005).
[8] N. Alem, R. Erni, C. Kisielowski, M. D. Rossell, W. Gannett, and A. Zettl, Phys. Rev. B **80**, 155425 (2009).
[9] R. M. Ribeiro and N. M. R. Peres, Phys. Rev. B **83**, 235312 (2011).
[10] L. Song, L. Ci, H. Lu, P. Sorokin, C. Jin, J. Ni, A. Kvashnin, D. Kvashnin, J. Lou, B. Yakobson, and P. Ajayan, Nano Lett. **10**, 3209 (2010).
[11] J. Serrano, A. Bosak, R. Arenal, M. Krisch, K. Watanabe, T. Taniguchi, H. Kanda, A. Rubio, and L. Wirtz, Phys. Rev. Lett. **98**, 095503 (2007).
[12] J. Petalas, S. Logothetidis, S. Boultadakis, M. Alouani, and J. M. Wills, Phys. Rev. B **52**, 8082 (1995).
[13] F. Litimein, B. Bouhafs, Z. Dridi, and P. Ruterana, New J. Phys. **4**, 64 (2002).
[14] P. D. Padova, C. Quaresima, C. Ottaviani, P. Sheverdyaeva, P. Moras, C. Carbone, D. Topwal, B. Olivieri, A. Kara, H. Oughaddou, B. Aufray, and G. L. Lay, Appl. Phys. Lett. **96**, 261905 (2010).
[15] J. P. Hague, Phys. Rev. B **84**, 155438 (2011).
[16] J. P. Hague, Nanoscale Res. Lett. **7**, 303 (2012).
[17] A. S. Alexandrov and P. E. Kornilovitch, J. Phys.: Condens. Matter **14**, 5337 (2002).
[18] M. Steiner, M. Freitag, V. Perebeinos, J. C. Tsang, J. P. Small, M. Kinoshita, D. Yuan, J. Liu, and P. Avouris, Nature Nanotechnol. **4**, 320 (2009).
[19] S. Fratini and F. Guinea, Phys. Rev. B **77**, 195415 (2008).
[20] L. Covaci and M. Berciu, Phys. Rev. Lett. **100**, 256405 (2008).
[21] N. V. Prokof'ev and B. V. Svistunov, Phys. Rev. Lett. **81**, 2514 (1998).
[22] A. S. Mishchenko, N. V. Prokof'ev, A. Sakamoto, and B. V. Svistunov, Phys. Rev. B **62**, 6317 (2000).
[23] J. P. Hague, J. Phys.: Conf. Ser. **286**, 012032 (2011).
[24] S. Fuchs, T. Pruschke, and M. Jarrell, Phys. Rev. E **81**, 056701 (2010).
[25] S. Nakajima, Y. Toyozawa, and R. Abe, *The Physics of Elementary Excitations*, Springer Series in Solid-State Sciences, Vol. 12 (Springer, Berlin, 1980).
[26] J. P. Hague and P. E. Kornilovitch, Phys. Rev. B **80**, 054301 (2009).
[27] J. P. Hague and P. E. Kornilovitch, Phys. Rev. B **82**, 094301 (2010).